

Nanoconnectomics

Terrence J. Sejnowski

Abstract The neuropil is a complicated 3D tangle of neural and glial processes. Recent advances in microconnectomics has made it possible to reconstruct neural circuits from serial-section electron microscopy at the micron scale. Electron microscopy allows even higher resolution reconstructions on the nanometer scale. Nanoconnectomic reconstructions approaching molecular resolution allow us to explore the topology of extracellular space and the precision with which synapses are modified by patterns of neural activity.

The reconstruction of a neural circuit is an essential step in understanding how signals are processed in the circuit; without this ‘wiring diagram,’ it is difficult to interpret the signals recorded from elements in the circuit. Connectomics attempts to reconstruct complete circuits, which can be accomplished at many spatial scales, as illustrated in Fig. 1. At the microconnectomic level, recent studies have focused on the retina (Kim et al., *Nature* 509:331–336, 2014) and the visual cortex (Bock et al., *Nature* 471:177–182, 2011). At the macroconnectomic level, the long-range cortical connections can be trace with diffusion tensor imaging (Van Essen, *Neuron* 80:775–790, 2013). This chapter will focus on nanoconnectomics, whose goal is to produce an accurate reconstruction of the neuropil at the nanometer scale.

Nanoconnectomics

At the level of nanometers, the neuropil is a tangled mass of synapses, dendrites, axons and glial cells surrounded by extracellular space. Each of these compartments contains specialized molecular structures for specialized functions and, in particular, those related to the processing of neural signals over a wide range of time

T.J. Sejnowski (✉)

Howard Hughes Medical Institute, The Salk Institute for Biological Studies, La Jolla, CA 92037, USA

Division of Biological Sciences, University of California at San Diego, La Jolla, CA 92093, USA

e-mail: terry@salk.edu

© The Author(s) 2016

H. Kennedy et al. (eds.), *Micro-, Meso- and Macro-Connectomics of the Brain*, Research and Perspectives in Neurosciences, DOI 10.1007/978-3-319-27777-6_1

Levels of Investigation

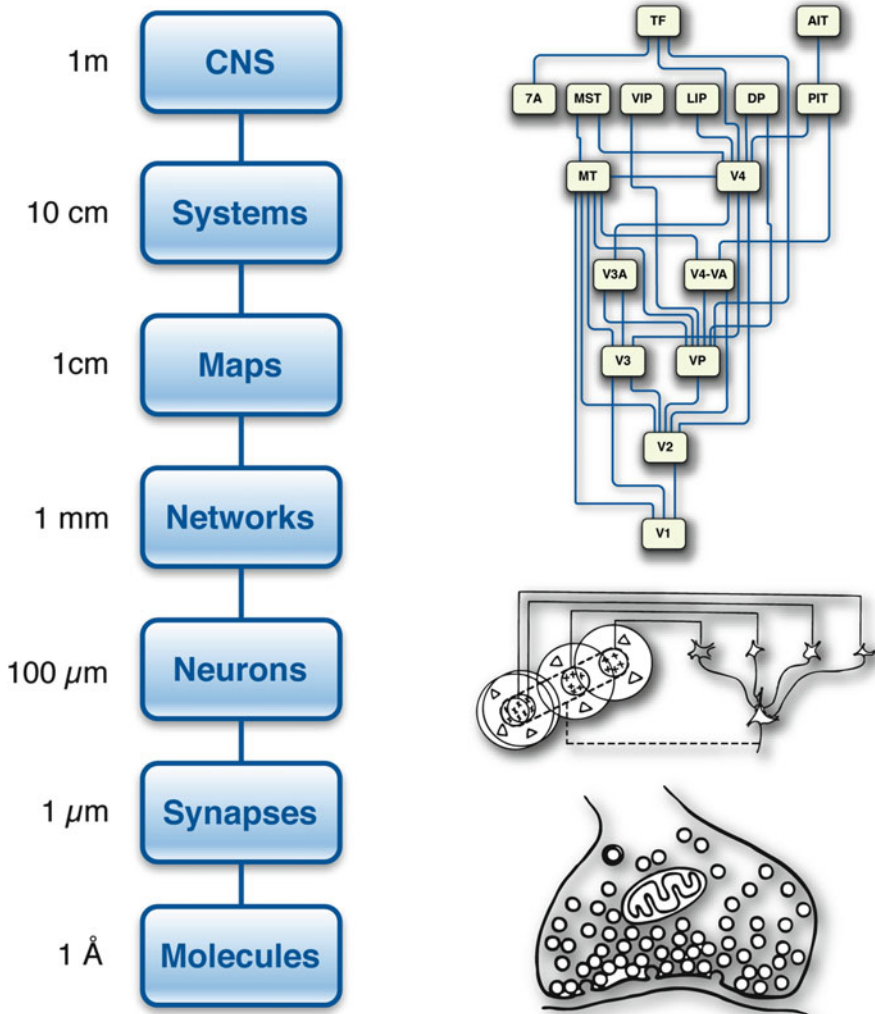


Fig. 1 Levels of investigation in the brain span 10 orders of spatial scale, from the molecular level to the entire central nervous system (CNS). Important structures and functions are found at each of these levels. Macroconnectomics provides the long-range connections between neurons in maps and systems, microconnectomics focuses on the network level, and nanoconnectomics extends down to synapses and molecules [adapted from Churchland and Sejnowski (1988)]

scales. We seek to reconstruct these compartments to understand the functions that are being implemented at the molecular level. Biochemistry is as important as electricity at these small spatial scales; at longer temporal scales beyond the second, biochemistry reigns supreme.

Biochemists typically carry out chemical reactions in test tubes, where the molecular reactants are well mixed and often in equilibrium. This approach makes spatial scales irrelevant, which is an advantage in measuring reaction rates and dissociation constants. In cells, however, strong concentration gradients exist on the nanoscale, and many important signaling pathways are not in equilibrium. Molecular signaling, such as the release of neurotransmitter at synapses or the entry of calcium into a dendritic spine, depends on changes in the concentration of the signaling molecules and is often transient, which may be on the microsecond time scale in nanovolumes and on much longer time scales in larger volumes.

Extracellular Space

To explore the consequences of transient neural signals in small volumes, a 3D $6 \times 6 \times 5 \mu\text{m}^3$ reconstruction of hippocampal neuropil was created via serial section transmission electron microscopy of tissue obtained from the middle of stratum radiatum in CA1 of hippocampus in an adult male rat (Mishchenko et al. 2010; Kinney et al. 2013). Although this was a relatively small volume of neuropil, within it there were 446 axons, 449 synapses, 149 dendritic branches and a small part of a single astrocyte. In addition, we took special care to reconstruct the extracellular space, which is an important compartment that is often neglected in reconstructions. Our goals were accuracy and completeness in order to serve as a test-bed for Monte-Carlo simulations of molecular cell signaling. However, there is much to be learned by just looking at the anatomy.

Imagine that the extracellular space was itself a compartment with its own geometry. What would it look like? Despite its importance for brain function, the morphology of the extracellular space (ECS) on the submicron scale is largely unknown. The ECS is tens of nanometers in width based on electron microscopy (EM) images (Thorne and Nicholson 2006), below the resolution of light microscopy. However, *in vivo* measurements of the ECS are available for the extracellular volume fraction, which captures the fraction of total tissue volume that lies outside of cells and the total tortuosity that accounts for the observed reduction in rate of diffusion of small molecules through the ECS compared to free diffusion due to geometric inhomogeneities and interactions with the extracellular matrix (Sykova and Nicholson 2008). In early development, the extracellular volume fraction is 40 % and decreases with age (Fiala et al. 1998) and during periods of anoxia (Sykova and Nicholson 2008). The extracellular volume fraction in the adult rat hippocampus is 20 % and total tortuosity is 1.45, based on the diffusion of small probe molecules in the ECS (Nicholson and Phillips 1981).

The processing of tissue for EM involves dehydration that results in tissue shrinkage, which reduces the extracellular space. To compensate for a range of possible volume shrinkages and *in vivo* variations, we explored quantitatively the range of physiological geometries of the ECS by rescaling the reconstruction (along three orthogonal dimensions), and we varied its lacunarity or ratio of the largest to the smallest membrane separations (Kinney et al. 2013). The reconstruction

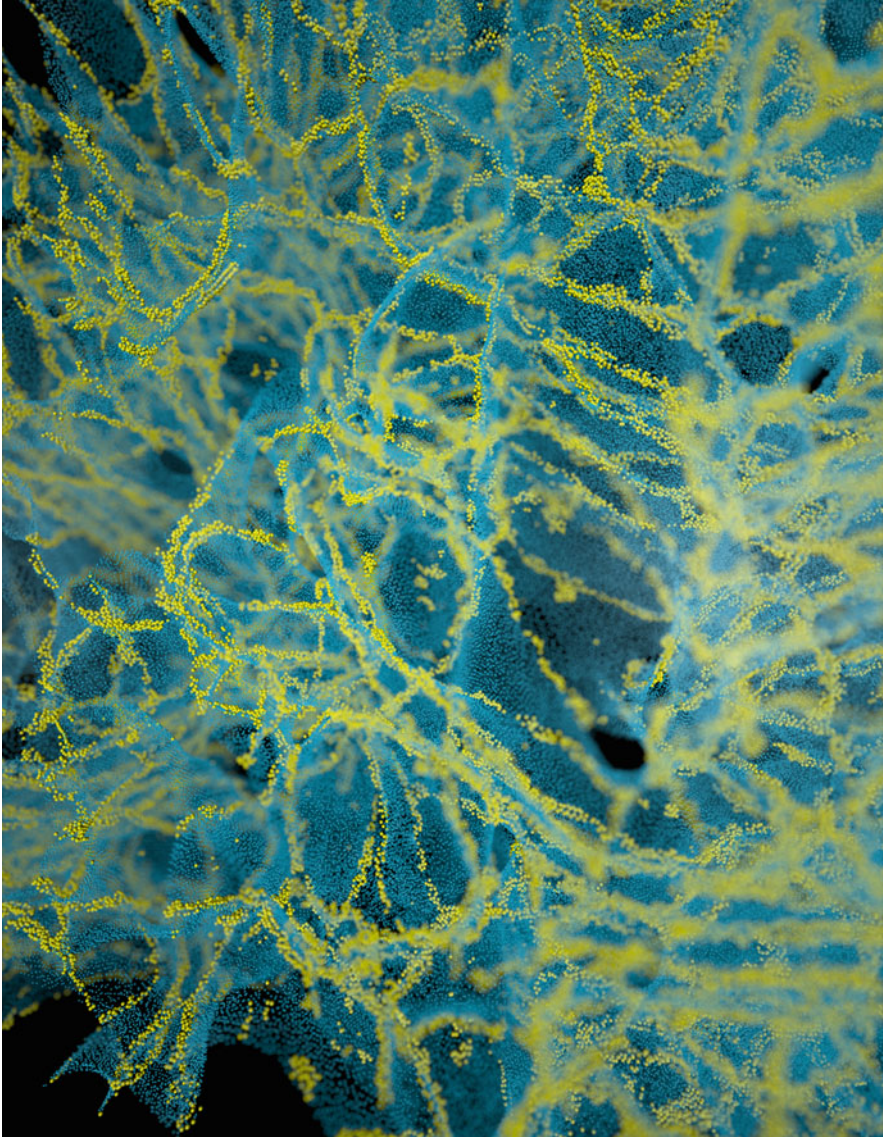


Fig. 2 Structure of the extracellular space between cells in the neuropil of the rat. In the reconstructed neuropil, 20–40-nm thick sheets (*blue dots*) separated pairs of cells and 40–80-nm tunnels occurred where three or more cells met (*yellow dots*). The topology of the extracellular space resembles that of soap bubbles [Justin Kinney]

revealed an interconnected network of 40–80-nm diameter tunnels, formed at the junction of three or more cellular processes and spanned by sheets between pairs of cell surfaces with 10–40 nm width. The tunnels tended to occur around synapses and axons, and the sheets were enriched around astrocytes. The intricate complexity of the ECS is shown in Fig. 2, which illustrates the geometry linking the sheets and

the tunnels. The non-uniformity found in the ECS may have specialized functions for signaling (sheets) and volume transmission (tunnels).

The ECS is a dynamic compartment and Fig. 2 should be considered a single snapshot. During sleep, for example, the extracellular volume increases by 60 %, allowing convective streaming to clear debris from the ECS (Xie et al. 2013).

Simulating Signaling in Small Spaces

Microdomains inside cells are small volumes, such as the femtoliter volumes of dendritic spines, in which concentrations of molecules can increase transiently and drive chemical reactions. We have simulated the transient release of neurotransmitters in the ECS and the entry of calcium into postsynaptic spines using MCell (mcell.org), a powerful and highly successful open source modeling tool for realistic simulation of cellular signaling in microdomains (Coggan et al. 2005; Nadkarni et al. 2012). At such small subcellular scales, macroscopic continuum assumptions do not apply and stochastic behavior dominates. MCell uses highly optimized Monte Carlo algorithms to track the stochastic behavior of discrete molecules in space and time as they diffuse and interact with other discrete effector molecules (e.g., ion channels, enzymes, transporters) heterogeneously distributed within the 3D geometry and on the 2D membrane surfaces of the subcellular environment. Monte Carlo methods are the best choice for reaction/diffusion simulation when the total number of interacting particles in a spatial domain is small, and/or when spatial particle gradients are steep. A further advantage of these methods is that, because individual particles are treated as reactive agents, reaction networks that exhibit combinatorial complexity can be described and simulated without simplification.

The postsynaptic density (PSD) in the active zone of a spine head contains hundreds of types of proteins in a large macromolecular complex. Because the PSD contains neurotransmitter receptors, the concentrations of ions in the PSD can transiently reach high concentrations briefly after receptor activation. For example, the volumes around voltage-dependent calcium channels are nanodomains, where calcium levels can reach concentrations that are several orders of magnitude higher than inside the spine (Tour et al. 2007). When calcium enters the spine head through NMDA receptors in the PSD, the calcium binds to calcium-binding proteins (Keller et al. 2008), which creates a strong gradient across the volume of the spine (Fig. 3). When calcium binds to calmodulin, one of the calcium-binding proteins, calmodulin can in turn bind to and activate calcium/calmodulin-dependent protein kinase II (CAMKII), which can lead to long-term potentiation of the synapse (Kennedy et al. 2005).

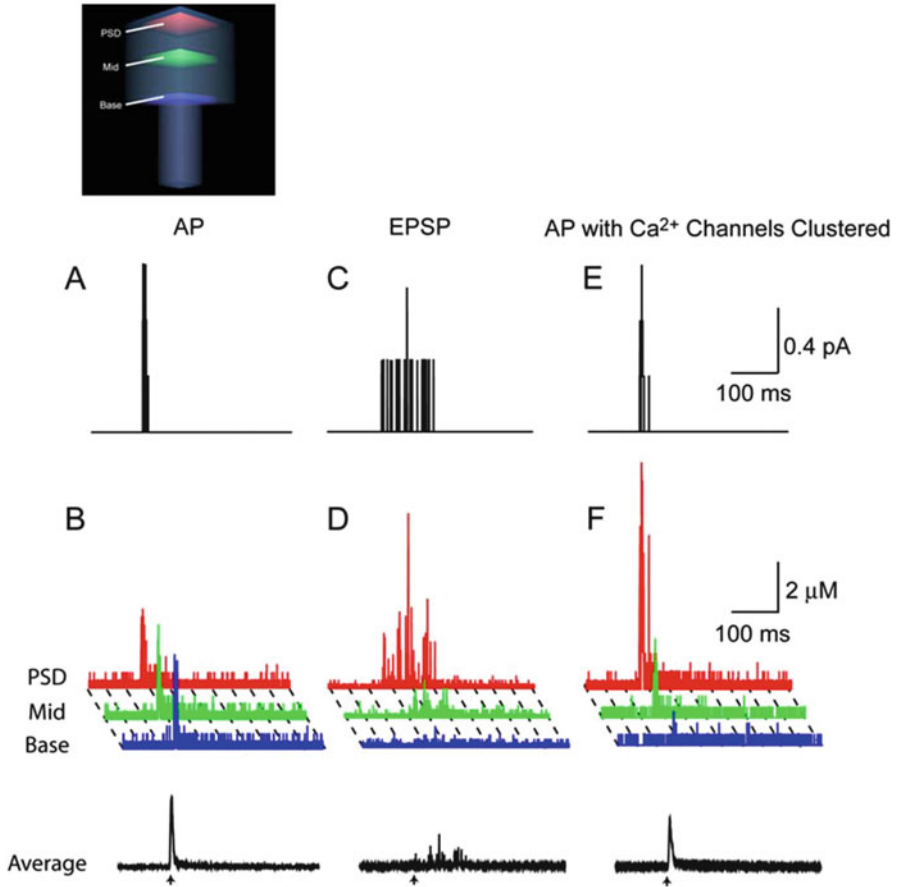


Fig. 3 Simulations of calcium entry into a spine and calcium gradients across the spine in the presence of 45 mM calbindin-D28k. Schematic (*upper left*) shows the spine subdivided into three distinct sampling regions: the postsynaptic density (PSD, *red*), the middle (MID, *green*), and the base (*blue*) of the spine. The volume averages are depicted below (*black*). (**a**) Instantaneous calcium current through voltage-dependent calcium channels in the spine during a back-propagating action potential (BAP). The time of somatic current injections is indicated by the *arrow*. (**b**) Calcium concentration in each of the three sampling regions is shown during the action potential. The colors of traces correspond to the three sampling regions shown in the schematic. Action potentials did not result in calcium gradients across the spine. The *black trace* at the *bottom* of the figure shows the volume-averaged $[Ca^{2+}]_i$ in the entire spine. (**c**) Instantaneous calcium current through NMDARs during an excitatory postsynaptic potential. (**d**) Calcium concentration in each of the three subregions of the spine during an excitatory postsynaptic potential as well as the volume average. Excitatory postsynaptic potentials resulted in large calcium gradients across the spine. (**e**) Open voltage-dependent calcium channels during an action potential simulation in which voltage-dependent calcium channels were clustered at the postsynaptic density. (**f**) Input-dependent calcium gradients across the spine during the BAP when the calcium channels were clustered in the PSD [adapted from Keller et al. (2008)]

Precision of Synaptic Plasticity

Excitatory synapses on dendritic spines of hippocampal pyramidal neurons have a wide range of sizes that are highly correlated with their synapse strengths (Harris and Stevens 1989). Pairs of spines on the same dendrite that received input from the same axon were of the same size and had nearly identical head volumes (Fig. 4). When plotted against one another, the paired head volumes were highly correlated with slope 0.91 and, despite the small sample size, were significantly different from random pairings of spines. In contrast, the spine neck volumes of the pairs were not well correlated, suggesting a different function.

Spine heads ranged in size over a factor of 60 from smallest to largest, allowing approximately 24 different strengths to be reliably distinguished across this range,

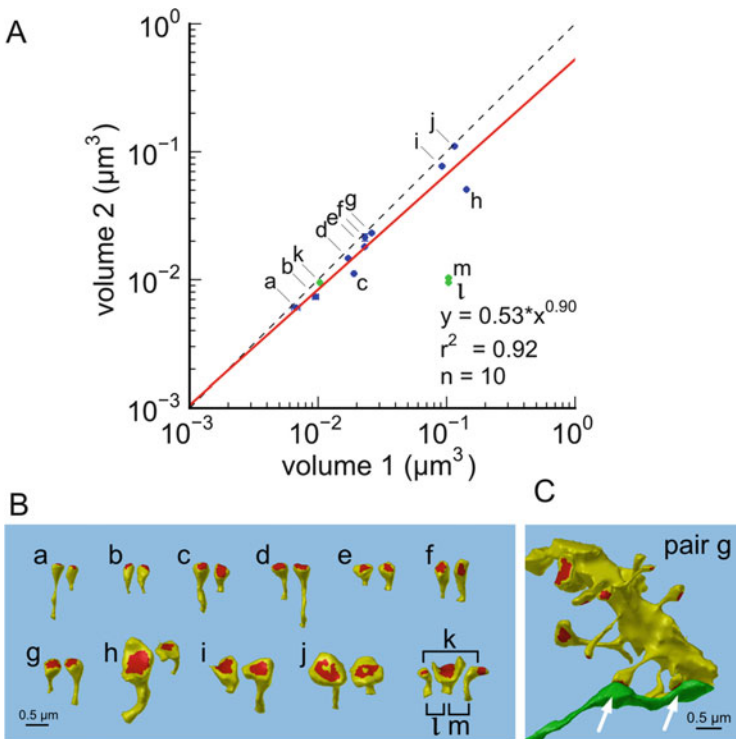


Fig. 4 Pairs of spines from the same axon on the same dendritic branch have highly correlated volumes. (A) Volumes of pairs of axonally coupled spines on the same dendritic branch plotted against one another (larger volumes on X axis, blue and green points, error bars show SEM). Labels a–m correspond to spine pairings in (B). Regression line of blue points is shown in red. Green points correspond to outlier pairings k, l, and m in (b). Dashed diagonal line represents line of perfect correlation. (B) Corresponding pairs of spines, isolated for visualization. (C) Example of a pair of axonally coupled spines on the same dendritic branch in situ. White arrows point to the spine heads [adapted from Bartol et al. (2015)]

assuming $CV = 0.083$ and a 75 % discrimination threshold. This corresponds to 4.6 bits of information that can be stored at each synapse (Bartol et al. 2015). The precision of the majority of smaller spines is as good as that of the minority larger spines (Fig. 4), suggesting that accurately maintaining the size of every synapse, regardless of size and strength, could be important for the function, flexibility and computational power of the hippocampus.

How can the high precision in spine head volume be achieved despite the many sources of stochastic variability observed in synaptic responses? Time-window averaging could smooth out fluctuations due to plasticity and other sources of variability. To set a lower bound on averaging time, we chose to examine neurotransmitter release probability as a single source of variability. Release can be analyzed using a binomial model in which n presynaptic action potentials, each with a probability p_r of releasing one or more vesicles, leads to a mean number of releases $m = n p_r$, having variance $\sigma^2 = n p_r (1 - p_r)$. The coefficient of variation around the mean is $CV = \text{sqrt}(\sigma^2)/m = \text{sqrt} [(1 - p_r)/(n p_r)]$ and can be compared with the measured values. Therefore, the number of spikes that are needed to reduce the variability to achieve a given CV is $n = (1 - p_r)/(p_r CV^2)$. Table 1 gives averaging time windows for representative values of p_r and a range of spiking rates of the presynaptic axon, which extends to many minutes for the smaller synapses. Accounting for other known sources of variability at dendritic spines would require even longer time windows.

Phosphorylation of CaMKII, which is required for some forms of synaptic plasticity, integrates calcium signals over 10–20 min and is a critical step in enzyme cascades leading to structural changes induced by long-term potentiation (LTP) and long-term depression (LTD; Kennedy et al. 2005), including rearrangements of the cytoskeleton (Kramár et al. 2012). The time course over which CaMKII integrates calcium signals is within the range of time windows that we predict would be needed for averaging (Table 1). Similar time windows occur in synaptic tagging and capture: inputs that are too weak to trigger LTP or LTD can be “rescued” by a stronger input to neighboring synapses if it occurs within an hour (Frey and Morris 1997; O’Donnell and Sejnowski 2014), which also requires CaMKII (Redondo and Morris 2011; de Carvalho Myskiw et al. 2014).

The reconstruction that we have analyzed is a tiny part of the hippocampus, but if it is representative, then the precision with which the spatial organization of the brain is constructed is at the nanolevel. Thus, evolution has optimized many of the structures at synapses that are essential for the long-term storage of information.

Table 1 Lower bounds on time window for averaging binomially distributed synaptic input to achieve $CV = 0.083$

Release probability (p_r)	Presynaptic spikes (n)	Averaging time (Rate = 1 Hz)	Averaging time (Rate = 25 Hz)
0.1	1306	21.8 min	52.2 s
0.2	581	9.68 min	23.2 s
0.5	145	2.42 min	5.8 s

In conclusion, nanconnectomics is revealing the extraordinary precision of synaptic plasticity and, together with Monte Carlo simulations of biochemical interaction and physiological responses, we can begin to see how the reactions between relatively small numbers of molecules in small volumes can accurately and efficiently create memories of past experiences.

Acknowledgments This research was supported by the Howard Hughes Medical Institute, the National Institutes of Health and the National Science Foundation. The neuropil reconstruction was a joint project with Kristen Harris, Chandra Bajaj and Justin Kinney and Thomas Bartol, Jr., who is the chief architect of MCell. Bartol, Mary Kennedy, Daniel Keller and Kevin Franks made important contributions to the simulations of calcium in spines heads.

Open Access This chapter is distributed under the terms of the Creative Commons Attribution-Noncommercial 2.5 License (<http://creativecommons.org/licenses/by-nc/2.5/>) which permits any noncommercial use, distribution, and reproduction in any medium, provided the original author(s) and source are credited.

The images or other third party material in this chapter are included in the work's Creative Commons license, unless indicated otherwise in the credit line; if such material is not included in the work's Creative Commons license and the respective action is not permitted by statutory regulation, users will need to obtain permission from the license holder to duplicate, adapt or reproduce the material.

References

- Bartol TM, Bromer C, Kinney JP, Chirillo MA, Bourne JN, Harris KM, Sejnowski TJ (2015) Hippocampal spine head sizes are highly precise. *BioRxiv*. doi: <http://dx.doi.org/10.1101/016329>
- Bock DD, Lee WC, Kerlin AM, Andermann ML, Hood G, Wetzel AW, Yurgenson S, Soucy ER, Kim HS, Reid RC (2011) Network anatomy and in vivo physiology of visual cortical neurons. *Nature* 471:177–182
- Churchland PS, Sejnowski TJ (1988) Perspectives on cognitive neuroscience. *Science* 242:741–745
- Coggan JS, Bartol TM, Esquenazi E, Stiles JR, Lamont S, Martone ME, Berg DK, Ellisman MH, Sejnowski TJ (2005) Evidence for ectopic neurotransmission at a neuronal synapse. *Science* 309:446–451
- de Carvalho Myskiw J, Furini CRG, Benetti F, Izquierdo I (2014) Hippocampal molecular mechanisms involved in the enhancement of fear extinction caused by exposure to novelty. *Proc Natl Acad Sci USA* 111:4572–4577
- Fiala JC, Feinberg M, Popov V, Harris KM (1998) Synaptogenesis via dendritic filopodia in developing hippocampal area CA1. *J Neurosci* 18:8900–8911
- Frey U, Morris RGM (1997) Synaptic tagging and long-term potentiation. *Nature* 385:533–536
- Harris KM, Stevens JK (1989) Dendritic spines of CA1 pyramidal cells in the rat hippocampus: serial electron microscopy with reference to their biophysical characteristics. *J Neurosci* 9:2982–2997
- Keller DX, Franks KM, Bartol TM, Sejnowski TJ (2008) Calmodulin activation by calcium transients in the postsynaptic density of dendritic spines. *PLoS ONE* 3(4):e2045
- Kennedy MB, Beale HC, Carlisle HJ, Washburn LR (2005) Integration of biochemical signalling in spines. *Nat Rev Neurosci* 6:423–434
- Kim JS, Greene MJ, Zlateski A, Lee K, Richardson M, Turaga SC, Purcaro M, Balkam M, Robinson A, Behabadi BF, Campos M, Denk W, Seung HS, EyeWriters (2014) Space-time wiring specificity supports direction selectivity in the retina. *Nature* 509:331–336

- Kinney JP, Spacek J, Bartol TM, Bajaj CL, Harris KM, Sejnowski TJ (2013) Extracellular sheets and tunnels modulate glutamate diffusion in hippocampal neuropil. *J Comp Neurol* 521:448–464
- Kramár EA, Babayan AH, Gavin CF, Cox CD, Jafari M, Gall CM, Rumbaugh G, Lynch G (2012) Synaptic evidence for the efficacy of spaced learning. *Proc Natl Acad Sci USA* 109:5121–5126
- Mishchenko Y, Hu T, Spacek J, Mendenhall J, Harris KM, Chklovskii DB (2010) Ultrastructural analysis of hippocampal neuropil from the connectomics perspective. *Neuron* 67:1009–1020
- Nadkarni S, Bartol TM, Stevens CF, Sejnowski TJ, Levine H (2012) Short-term plasticity constrains spatial organization of a hippocampal presynaptic terminal. *Proc Natl Acad Sci USA* 109:14657–14662
- Nicholson C, Phillips JM. (1981) Ion diffusion modified by tortuosity and volume fraction in the extracellular microenvironment of the rat cerebellum. *J Physiol* 321:225–257
- O'Donnell C, Sejnowski TJ (2014) Selective memory generalization by spatial patterning of protein synthesis. *Neuron* 83:398–412
- Redondo RL, Morris RGM (2011) Making memories last: the synaptic tagging and capture hypothesis. *Nat Rev Neurosci* 12(1):17–30
- Sykova E, Nicholson C (2008) Diffusion in brain extracellular space. *Physiol Rev* 88:1277–1340
- Thorne RG, Nicholson C (2006) In vivo diffusion analysis with quantum dots and dextrans predicts the width of brain extracellular space. *Proc Natl Acad Sci USA* 103:5567–5572
- Tour O, Adams SR, Kerr RA, Meijer RM, Sejnowski TJ, Tsien RW (2007) Calcium-green-FIAsH: a genetically targeted small molecule calcium indicator. *Nat Chem Biol* 3:423–431
- Van Essen DC (2013) Cartography and connectomes. *Neuron* 80:775–790
- Xie L, Kang H, Xu Q, Chen MJ, Liao Y, Thiyagarajan M, O'Donnell J, Christensen DJ, Nicholson C, Iliff JJ, Takano T, Deane R, Nedergaard M (2013) Sleep drives metabolite clearance from the adult brain. *Science* 342:373–377